International Journal of Control and Automation
Vol. 8, No. 1 (2015), pp. 251-262
http://dx.doi.org/10.14257/ijca.2015.8.1.23

Study on the Flow Characteristics and Erosion Phenomenon of Frac Sleeve by Using a CFD Approach

Chao Zheng[1], Yonghong Liu*[1], Hanxiang Wang[1], Renjie Ji[1], Zengkai Liu[1], Shilin Yu[2] and Bei Wang[3]

[1]*College of Mechanical and Electronic Engineering, China University of Petroleum, Qingdao 266580, China*
[2]*CNOOC Energy Technology & Services-Human Resources Co., Tianjin 300456, China*
[3]*Rongsheng Machinery Manufacture Ltd. of Huabei Oilfield, Renqiu 062550, China*
zhengchaoupc@163.com, liuyhupc@163.com, wanghx1899@163.com, jirenjie@163.com, liuzengk@163.com, yushilin1988@sina.com, emily_ysu@163.com

Abstract

The fracturing technology has been widely applied to break up the formation in oil & gas industry. The flow dynamics and erosion phenomenon of frac sleeve in fracturing process is important but has not been studied previously. In this paper, the dynamics is studied numerically with special reference to the effect of sand mass flow rate. The simulation is conducted using a coupled approach of Computational Fluid Dynamics and Discrete Element Method. The influence of port parameters such as shape, size and number arrangement on the erosion rate was investigated. Based on this study, motion characteristics of fracturing fluid and sand particles are obtained, the structure parameters can be optimized. The frac sleeve after structural optimization obtains better erosion resistance. This study shows that Computational Fluid Dynamics could be a useful tool to study the dynamics and internal flow of fracturing tool.

Keywords: *Erosion, Frac sleeve, Fracturing, Computational Fluid Dynamics*

1. Introduction

Fracturing is a well-stimulation method which injects water, sand and chemicals deeply into ground to break up the formation and release oil & gas [1-2]. The erosion phenomenon is one of typical problems which are frequently encountered in fracturing process [3]. During the fracturing process, fracturing fluid containing sand as proppant is pumped to downhole. Fracturing technology has a range of features such as high pressure, high sand rate and high flow rate， which may cause the erosion phenomenon of tool where people have paid great attention to. The frac sleeve is a special tool used to inject fracturing fluid into reservoir formation [4].

The inner flow status of frac sleeve which has a significant relationship with the shape characteristic is complex. Inappropriate design of frac sleeve may lead to serious vortex phenomenon of fracturing fluid, which contributes to the high erosion rate [5]. As is known, the erosion phenomenon of fracturing tool is a complex problem closely related to density, sand flow rate, sand content and shape of sand. It is very difficult to measure the internal flow status and movement of sand particles downhole. Without such microscopic information, downhole fracturing is largely operated as a black-box operation. In order to study the erosion problem, a coupled Computational Fluid Dynamics (CFD) approach which is mainly used in initial studies in connection with Lagrangian particle tracking

ISSN: 2005-4297 IJCA

model is introduced to simulate the movement characteristics of fracturing fluid and sand particles [6-9]. The majority of the previous studies were devoted to material characteristics, while little attention had been paid to the characteristics of fracturing fluid and sand particles. A lot of researches have been conducted on erosion phenomenon in other industrial [10-15]. The coupled approach of CFD and Discrete Element Method is used to simulate the solid-liquid two phase flow [16-18]. In these studies, particles are modeled as a kind of discrete phase, while the fluid is treated as a kind of continuous phase. The approach has been recognized as an effective method to study the characteristics of solid-liquid flow by various investigators [19-20].

In this paper, in order to enrich the understanding of erosion phenomenon in fracturing operation, downhole flow characteristics and erosion phenomenon are investigated by using a CFD approach. To get the relationship between erosion rate and tool shape, models with different parameters are created and analyzed. Based on the analysis and optimization of port which is arranged on tool surface, frac sleeve with better erosion resistance can be obtained.

2. Simulation Method

2.1. Turbulence Model

To simulate internal flow of fracturing liquid and motion of solid particles in the frac sleeve correctly, proper turbulence models should be offered to describe the flow of fracturing fluid [19]. The downhole surrounding is unsteady and complicated. In the computational fluid dynamics, turbulence models are offered to control vortex phenomenon and flow status. Taking the Reynolds number and solving ability into account, the standard k-ε model is a proper choice to describe flow status. The turbulence equations are listed as:

$$\rho u_j \frac{\partial k}{\partial x_j} = \frac{\partial}{\partial x_i}\left[\left(\eta + \frac{\eta_t}{\sigma_k}\right)\frac{\partial k}{\partial x_j}\right] + \eta_t \frac{\partial u_i}{\partial x_j}\left(\frac{\partial u_i}{\partial x_j} + \frac{\partial u_j}{\partial x_i}\right) - \rho\varepsilon \tag{1}$$

$$\rho u_k \frac{\partial \varepsilon}{\partial x_k} = \frac{\partial}{\partial x_k}\left[\left(\eta + \frac{\eta_t}{\sigma_\varepsilon}\right)\frac{\partial \varepsilon}{\partial x_k}\right] + \frac{C_1\varepsilon}{k}\eta_t \frac{\partial u_i}{\partial x_j}\left(\frac{\partial u_i}{\partial x_j} + \frac{\partial u_j}{\partial x_i}\right) - C_2\rho\frac{\varepsilon^2}{k} \tag{2}$$

$$\eta_t = C_\mu \rho k^2 / \varepsilon \tag{3}$$

Where ρ is fluid density, μ is kinematic viscosity, k is turbulent kinetic energy, u is average velocity, ε is dissipation rate and η_t is turbulent viscosity.

In the turbulence equation, according to recommended values by previous researchers, values of coefficients and constants are shown as: C_1=0.09, C_2 =1.44, C_μ= 1.92, σ_k=1.0, σ_ε=1.3.

2.2. Particle Trajectory

Discrete phase model is a kind of particle trajectory model which uses Lagrangian method to treat fracturing fluid as continuous phase and regards solid particles as discrete phase. In addition, there is a relative slip between the solid phase and the continuous phase [20]. Firstly, the flow field of fracturing fluid is calculated and the particle phase is applied in the Euler coordinate system. Then the trajectory of solid particles is tracked in the Lagrangian coordinate system.

In the Lagrangian coordinate system, trajectories of particles can be solved by integrating the force equations, which can be written as:

$$\frac{du_{p,i}}{dt} = F_D(u_i - u_{p,i}) + \frac{\rho_p - \rho}{\rho_p} g_i + F_i \tag{4}$$

Where u_p 、 u are velocity of solid phase and continuous phase, respectively; $F_D(u_i - u_{p,i})$ is drag force of i direction for per unit mass of particles:

$$F_D = \frac{18\mu}{\rho_p d_p^2}\frac{C_D \mathrm{Re}_p}{24} \tag{5}$$

Where μ is viscosity of fluid; ρ is density of fluid, ρ_p is density of particles, d_p is diameter of particles and Re_p is Reynolds number which can be expressed as:

$$\mathrm{Re}_p = \frac{\rho d_p \left|u_p - u\right|}{\mu} \tag{6}$$

The Drag force coefficient of the particles (C_D) can be calculated by the following formula:

$$C_D = \begin{cases} \dfrac{\mathrm{Re}_p}{24} & \mathrm{Re}_p \le 1 \\ \dfrac{\mathrm{Re}_p}{24}(1.0 + \dfrac{1}{6}\mathrm{Re}_p^{2/3}) & 1 < \mathrm{Re}_p \le 1000 \\ 0.424 & \mathrm{Re}_p > 1000 \end{cases} \tag{7}$$

After simplifying the formula (1-1), momentum equation of particle can be obtained:

$$\frac{du_{p,i}}{dt} = \frac{1}{\tau_p}(u_i - u_{p,i}) - g \tag{8}$$

Where τ_p is relaxation time.

Moreover, trajectory of particle is affected by the pulsation of fracturing fluid:

$$u = \bar{u} + u' \tag{9}$$

Adding formula (9) into (8), momentum equation of particle can be expressed as:

$$\frac{du_{p,i}}{dt} = \frac{1}{\tau_p}(\bar{u}_i - u_i' - u_{p,i}) \tag{10}$$

In cylindrical coordinates, momentum equation can be also expressed as:

$$\frac{du_p}{dt} = \frac{1}{\tau_p}(\bar{u} + u' - u_p) - \frac{u_p v_p}{r} \tag{11}$$

$$\frac{dv_p}{dt} = \frac{1}{\tau_p}(\bar{v} + v' - v_p) + \frac{u_p^2}{r} \tag{12}$$

$$\frac{dw_p}{dt} = \frac{1}{\tau_p}(\bar{w} + w' - w_p) - g \tag{13}$$

Where u_p, v_p and w_p are radial, tangential and axial velocity of particle, respectively; $\bar{u}$, $\bar{v}$ and $\bar{w}$ are radial, tangential and axial velocity of continuous phase, respectively; u', v' and w' are radial, tangential and axial pulsation velocity of continuous phase, respectively.

2.3. Erosion Calculation

According to references, different models have been investigated to solve erosion problem. In these models, erosion equation is the core element. Erosion phenomenon attributes to the impact of sand particles and tool surface. In erosion equation, parameters such as impact velocity, impact angle and impact number of particles will contribute an important effect to erosion rate. Above all, the erosion equation is defined as:

$$R_{erosion} = \sum_{p=1}^{N_{Particles}} \frac{\dot{m}_p C(d_p) f(\alpha) V_p^{b(V_p)}}{A_{face}} \quad (14)$$

Where, $C(d_p)$ is function of the particle size; α is impact angle between surface and particles; $f(\alpha)$ is function associated with impact angle; V_p is particle impact velocity; $b(V_p)$ is a function related to particle impact velocity; A_{face} is area of calculation unit; $\dot{m}_p$ is mass flow rate of particles in the calculation; $N_{particles}$ is the number of particles impact on area A_{face}; $R_{erosion}$ is erosion rate and the unit is kg/(m^2·s).

3. Numerical Simulation

3.1. Working Principle

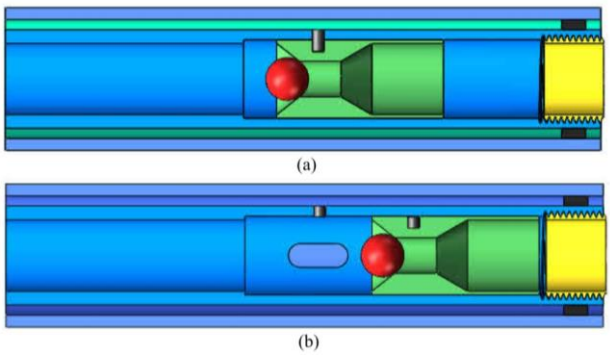

Figure 1. Schematic Diagram for Fracturing System (a) Close Position, (b) Open Position

In this study, the fracturing system is introduced and the working principle is shown in Figure 1. The fracturing system mainly contains frac sleeve, casing, packer, lock pin, ball and ball seat. There are two statuses for the fracturing system: frac sleeve is in close position before the ball is dropped as shown in Figure 1 (a); frac sleeve is in open position after ball is dropped as shown in Figure 1 (b). During fracturing process, fracturing fluid flows into concentric annulus, then flows upper, until flows into formation through perforation section. The position of perforation section has a long distance away from ports. Considering the limit of calculation resource, the simulated filed should be chose and simplified properly.

3.2. Mesh Generation

Figure 2 shows the mesh of frac sleeve geometry. As world's most popular CFD software, Fluent is widely used in the aerospace, automotive design and other fields for its extensive physical models, advanced numerical methods and powerful preprocessor and postprocessor function. Due to these features, it is chose for this study. To get more accurate simulation results, meshes with high quality should be adopted. The Gambit which is also developed by the Fluent Inc is chose to preprocess the geometry, here follows the meshing result.

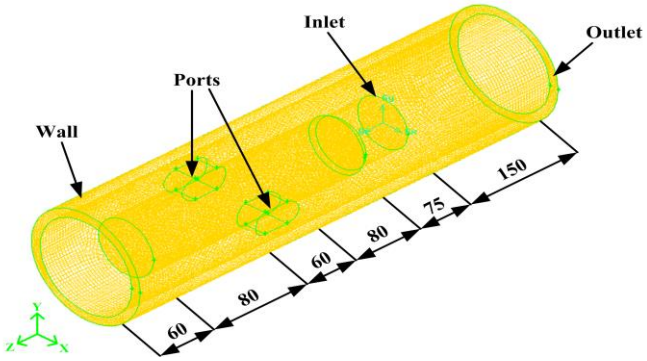

Figure 2. Mesh of the Frac Sleeve Geometry

3.3. Calculation Conditions

Calculation conditions are given in Table 1. Parameters listed in the table provide initial conditions for solving the flow field. These parameters such as flow rate, density and viscosity can affect flow status of fracturing fluid obviously. The Computational Fluid Dynamics provides the convenient and appropriate model to solve this problem. After iteration, movement information of fracturing fluid and sand particles can be achieved.

Table 1. Calculation Conditions

Parameter	Value	Unit
Flow rate	4.5	m^3/min
Density of liquid	1100	kg/m^3
Viscosity of liquid	100	mPa·s
Density of sand	2300	kg/m^3
Diameter of sand	380	Mm
Sand flow rate	12	kg/s

4. Simulation Results and Discussion

4.1. Characteristics of Flow Field

Figure 3 (a) shows the overall view of velocity vector of plane Y=0 and Figure 3 (b) shows the partial enlarged view of port area. It is clearly shown that velocity is small and uniform at the entrance, but large at the port area. Vortex and backflow can be seen in the partial enlarged view, which means that flow status change dramatically at the port. The velocity of fracturing fluid at the entrance is nearly 20m/s, while reaching up to 60m/s at the port area. It is because that flow channel which narrows rapidly at port area leads to change of flow status. The biggest value of gradient change appears at the port. Furthermore, existence of vortex and backflow leads to erosion phenomenon of port area.

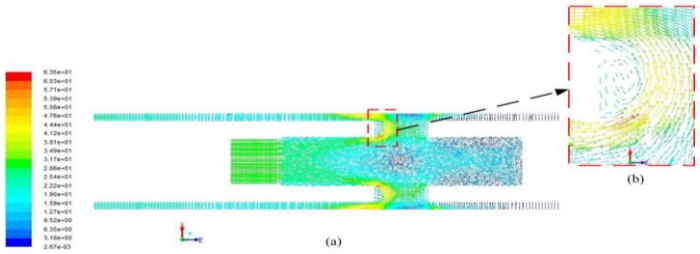

Figure 3. Velocity Vector of Flow Field
(a) Velocity Vector of Plane (Y=0), (b) Zoom of Velocity Vector at Port Area

Figure 4 shows the pressure contour of plane (Y=0). From the Figure, it can be seen that pressure at entrance is 31.1Mpa and reduces to 30.0Mpa at the exit. The factors leading to the pressure loss include friction between fracturing fluid and wall surface, collisions between particles and wall surface and the inner friction of fracturing fluid. The interaction of these factors contributes to pressure loss when the fracturing fluid flows from entrance to exit. From the pressure contour, it can be seen that the pressure has an inversely proportional relationship with velocity at the port area. This phenomenon is in line with Bernoulli's law.

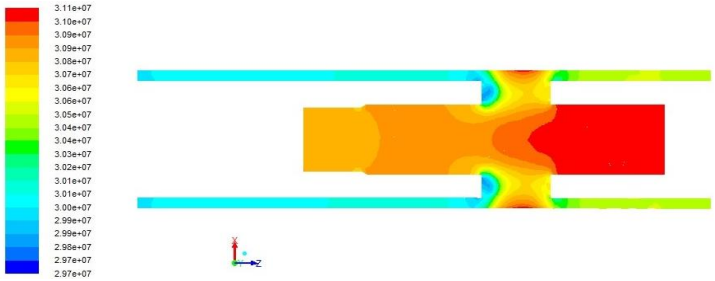

Figure 4. Pressure Contour of Plane (Y=0)

Figure 5 shows trajectories of sand particles. In fracturing process, sand particles are carried by fracturing fluid. It is obvious to see that fluctuations and uncertainty of trajectories exist. This is because that sand particles are affected by various forces such as Gravity force, Drag force, Pressure gradient force, Buoyancy force and Added mass force. The interactions of these forces lead to fluctuations and uncertainty of trajectories.

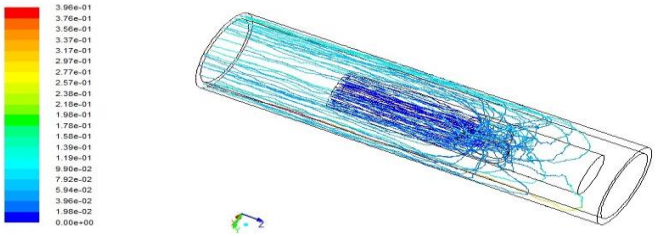

Figure 5. Trajectories of Sand Particles

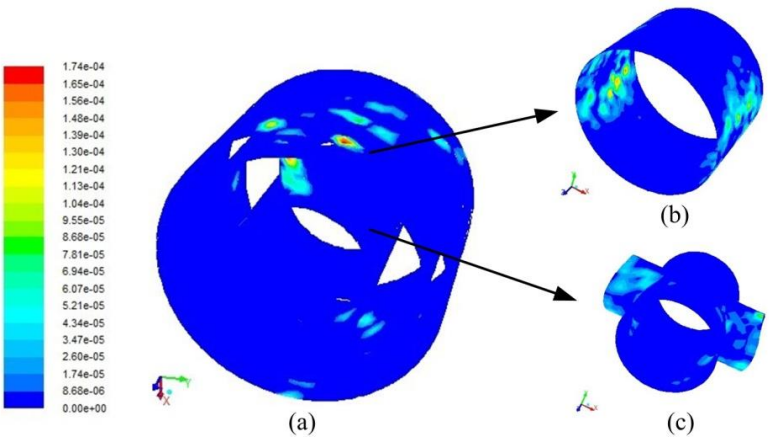

Figure 6. Erosion Contour on the Surface of Tool (a) Overall Erosion Contour; (b) Erosion Contour on Surface of Casing; (c) Erosion Contour at Port Area

Figure 6 (a) shows overall erosion contour of tools, Figure 6 (b) shows the erosion contour of casing and Figure 6 (c) shows the erosion contour at port area. From erosion contour, it is clear to see that inner surface of casing and the inner surface of ports are high erosion areas. It can be explained that sand particles impact sharply at these areas.

4.2. Effects of Port Shape

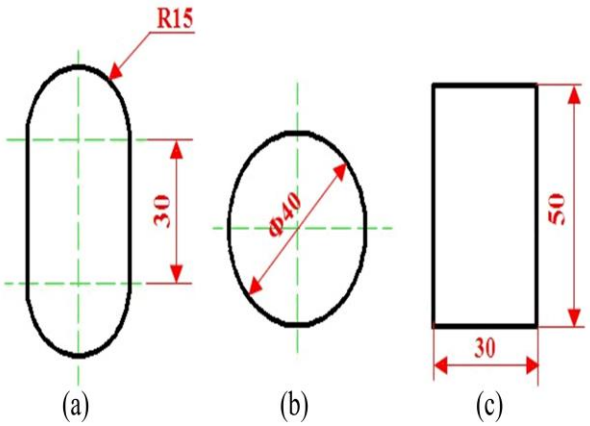

Figure 7. Schematic Diagram of Different Shape

To investigate the effect of port shape on erosion rate, models with different shapes, sizes and numbers are studied. Figure 7 shows different shapes of port labeled with parameters. To simplify calculation, models with Z axis value between 140mm and 230mm are chose for the object section. The average erosion of object section is compared and analyzed.

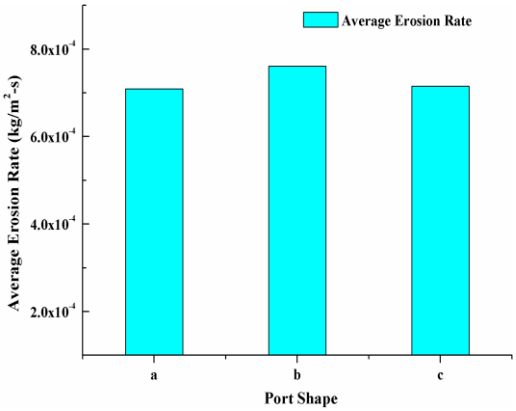

Figure 8. Effect of Port Shape on the Average Erosion Rate

Figure 8 shows the comparison of average erosion rate. From Figure 8, it can be found that the model with shape a (ellipse) has the lowest average erosion rate, while the model with shape b (rectangle) has the highest erosion rate. So the model with ellipse shape has better erosion resistance. It can be explained that flow status of model with ellipse shape is better and the movement of sand particles are relatively stable, resulting in the low erosion rate of fracturing tools.

4.3. Effects of Port Size

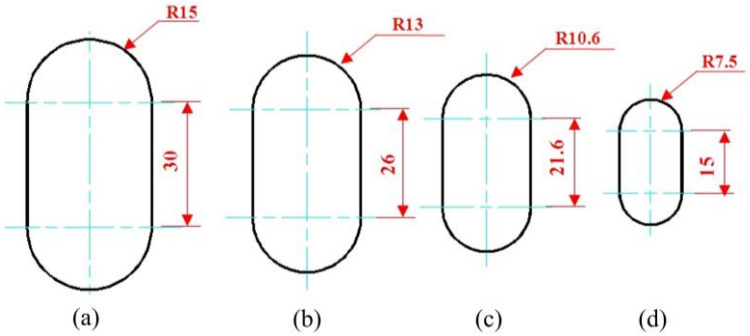

Figure 9. Schematic Diagram of Different Size (a) 3200mm2, (b) 2400mm2, (c) 1600mm2, (d) 800mm2

To study the effect of size on erosion rate, four models with different port sizes are set respectively, while keeping other dimensions unchanged. Figure 9 shows the schematic diagram of four models with different size. The size of port can affect flow status of fracturing fluid significantly.

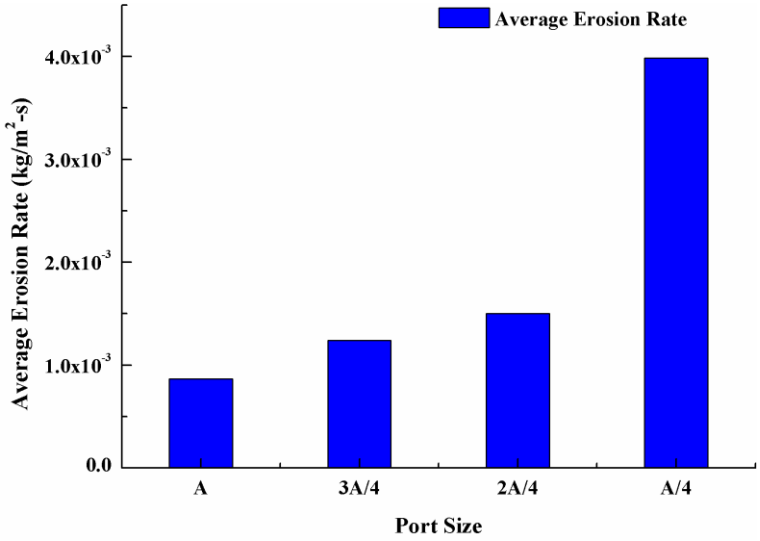

Figure 10. Effect of Port Size on the Average Erosion Rate

Figure 10 shows the comparison of average erosion rate of four kinds of size. From the histogram, it is clear to see that erosion rate shows exponential growth with size of ports decrease. The model with size A (3200mm^2) has the lowest erosion rate, while the model with size A/4 (800mm^2) has the highest erosion rate.

Figure 11 shows sand trajectories of models with different port size. The trajectory reflects collisions between sand particles wall surface during the transportation. At the same time, it also reflects flow status of fracturing fluid. The more disorder the motion of fracturing fluid is, the more disorder the trajectory of sand is. In Figure 11, it can be found that trajectories of Figure 11 (a) are relatively close to Figure 11 (b). When size of port narrows continuously, trajectories become more disorder. In Figure 11 (d), it is clear to see that sand particles appear cyclotron motion. This indicates that collision at the port area is very fierce. This phenomenon also confirms previous simulation results.

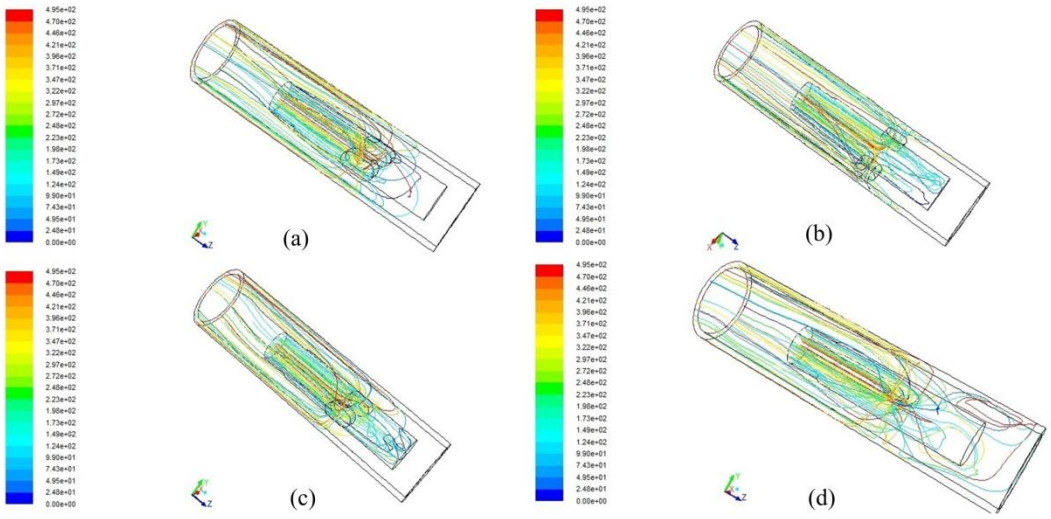

Figure 11. Sand Trajectories of Models with Different Port Size (a) 3200mm2, (b) 2400mm2, (c) 1600mm2, (d) 800mm2

4.4. Effects of Port Number

According to actual usage, port performs the diversion function. The number of port affects the diversion function. Keeping same total area of ports, models with two ports, four ports, six ports and eight ports are calculated and analyzed. Figure 12 shows the schematic diagram of models with different port number.

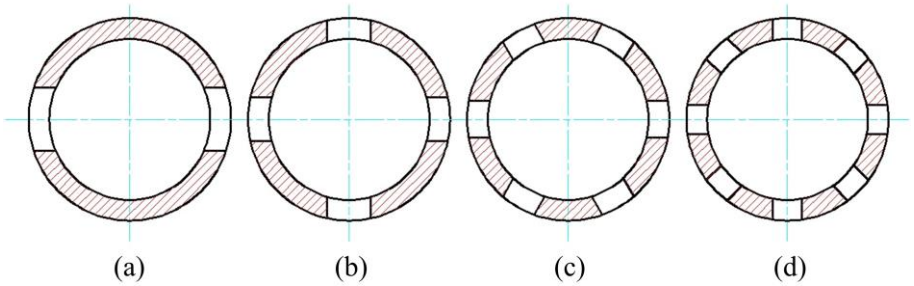

Figure 12. Schematic Diagram of Different Port Number (a) Two Ports, (b) Four Ports, (c) Six Ports, (d) Eight Ports

In order to investigate the influence of port number on erosion rate, an average erosion rate histogram was drew and shown in Figure 13. From the histogram, it can be seen that average erosion rate decreases with port number increase. The average erosion rate of two, four, six and eight ports model is 8.62×10^{-4} kg/(m^2·s), 6.11×10^{-4} kg/(m^2·s), 3.14×10^{-4} kg/(m^2·s)and 3.36×10^{-4} kg/(m^2·s), respectively.

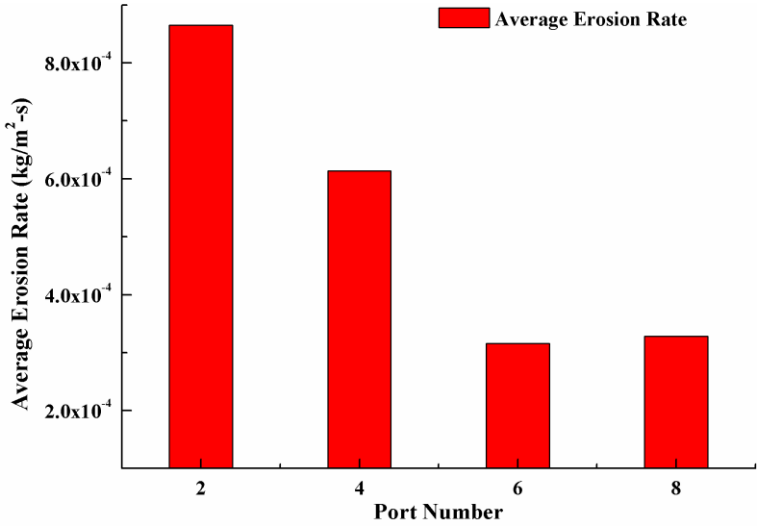

Figure 13. Effect of Port Number on the Average Erosion Rate

Thus, the average erosion rate shows a decreasing trend with port number increase. For two ports model, the average erosion rate is the largest, while average erosion rate of six ports model is the smallest. Which illustrates the increase of port number can improve flow status of fracturing fluid.

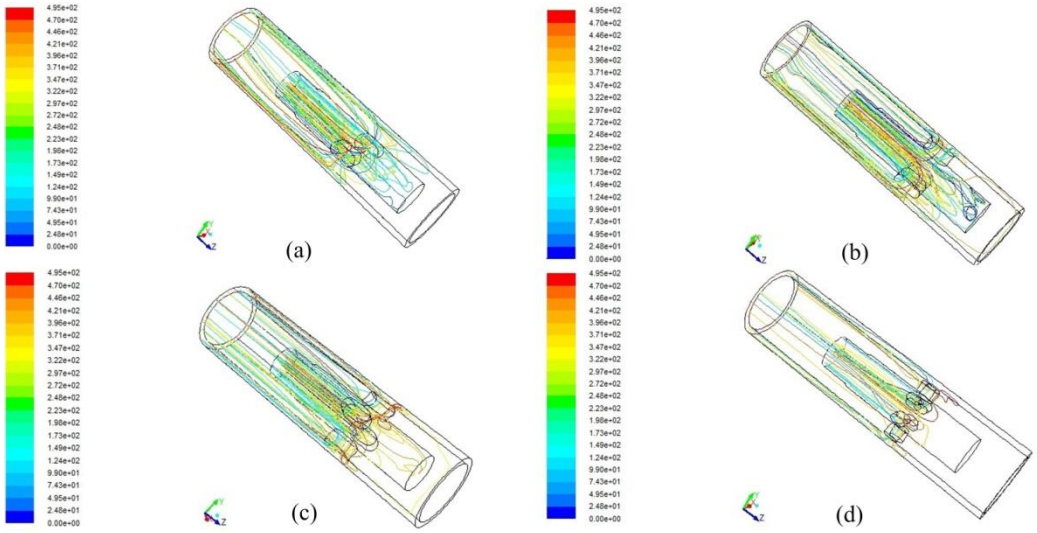

Figure 14. Sand Trajectories of Different Number
(a) Two Ports, (b) Four Ports, (c) Six Ports, (d) Eight Ports

Figure 14 shows sand trajectories of models with different port number. For two ports and four ports model, sand trajectories are more complex and unstable. For six ports and eight ports model, sand trajectories are more gradual. This is because that flow status of fracturing fluid is improved with port number increases. This also explains the reason why an increase in port number can decrease average erosion rate of tool.

5. Conclusions

This study performs a CFD analysis including flow field characteristics and erosion phenomenon. Models with different parameters are established and analyzed. Based on the comprehensive study, the following conclusions could be achieved:

(1) Due to the narrowing of flow channel, large velocity and pressure gradient generate at port area. The maximum velocity of fracturing fluid and sand particles is also located at the port, and the peak erosion rate is found at inner surface of ports and casing.

(2) The shape and size of port has a significant influence on the motion characteristics of fracturing fluid and sand particles. The ellipse shape contributes to a better flow status and erosion resistance. The motion of fracturing fluid and sand particles becomes fierce.

(3) The effect of port number on erosion rate is also studied. Keeping the total area of ports unchanged, increase of port number can slow down velocity of fracturing fluid and impinging between sand and surface. These results can be instructive to the design of frac sleeve.

Acknowledgements

This paper is a revised and expanded version of a paper entitled [Numerical Simulation of Downhole Completion Equipment via Computational Fluid Dynamics] presented at [The 3rd International Conference on Next Generation Computer and Information Technology, Hochimin, October 24-26, 2014]. The authors wish to acknowledge the support provided by the National Natural Science Foundation of China (No. 51205411), the Shandong Provincial Natural Science Foundation of China (No. ZR2012EEL15), National High-Technology Research and Development Program of China (No.2013AA09A220), and Taishan Scholar project of Shandong Province (TS20110823).

References

[1] M. Gu and K. K. Mohanty, "Effect of foam quality on effectiveness of hydraulic fracturing in shales", Int. J. Rock Mech. Min. Sci., vol. 70, **(2014)**, pp. 273-285.
[2] L. Zhou, M. Z. Hou and Y. Gou, "Numerical investigation of a low-efficient hydraulic fracturing operation in a tight gas reservoir in the North German Basin", J. Pet. Sci. Eng., vol. 120, **(2014)**, pp. 119-129.
[3] L. Thakur and N. Arora, "A comparative study on slurry and dry erosion behaviour of HVOF sprayed WC-CoCr coatings", Wear, vol. 303, **(2013)**, pp. 405-411.
[4] C. Maurer and U. Schulz, "Solid particle erosion of thick PVD coatings on CFRP", Wear, vol. 317, **(2014)**, pp. 246-253.
[5] Z. G. Liu, S. Wan and V. B. Nguyen, "A numerical study on the effect of particle shape on the erosion of ductile materials", Wear, vol. 313, **(2014)**, pp. 135-142.
[6] M. S. Saidi, M. Rismanian, M. Monjezi, M. Zendehbad and S. Fatehiboroujeni, "Comparison between Lagrangian and Eulerian approaches in predicting motion of micron-sized particles in laminar flows", Atmos. Environ., vol. 89, **(2014)**, pp. 199-206.
[7] L. Gurreri and A. Tamburini, "CFD prediction of concentration polarization phenomena in spacer-filled channels for reverse electrodialysis", J. Membr. Sci., vol. 468, **(2014)**, pp. 133-148.
[8] D. C. Cohen Stuart, C. R. Kleijn and S. Kenjereš, "An efficient and robust method for Lagrangian magnetic particle tracking in fluid flow simulations on unstructured grids", Comput. Fluids, vol. 40, **(2011)**, pp. 188-194.
[9] C. Zheng, Y. H. Liu, H. X. Wang, R. J. Ji and Z. K. Liu, "Numerical Simulation of Downhole Completion Equipment via Computational Fluid Dynamics", Proceedings of the 3rd International Conference on Next Generation Computer and Information Technology, **(2014)**; Hochimin, Vietnam.
[10] J. R. Laguna-Camacho, A. Arquina-Chavez, J. V. Méndez-Méndez, M. Vite-Torres and E. A. Gallardo-Hernández, "Solid particle erosion of AISI 304, 316 and 420 stainless steel", Wear, vol. 301, **(2013)**, pp. 398-405.
[11] C. Y. Wong, C. Solnordal and A. Swallow, "Experimental and computational modelling of solid particle erosion in a pipe annular cavity", Wear, vol. 303, **(2013)**, pp. 109-129.
[12] M. Atkinson, E. V. Stepanov, D. P. Goulet, S. V. Sherikar and J. Hunter, "High pressure testing sand erosion in 3D flow channels and correlation with CFD", Wear, vol. 263, **(2007)**, pp. 270-277.
[13] X. G. Song, J. H. Park and S. G. Kim, "Performance comparison and erosion prediction of jet pumps by using a numerical method", Math. Comput. Model., vol. 57, **(2013)**, pp. 245-253.
[14] X. C. Wang, J. G. Zhang and F. H. Sun, "Investigations on the fabrication and erosion behavior of the composite diamond coated nozzles", Wear, vol. 304, **(2013)**, pp. 126-137.
[15] T. Karthikeyan, S. John Peter and S. Chidambaranathan, "Hybrid Algorithm for Noise-free High Density Clusters with Self-Detection of Best Number of Clusters", Int. J. Hybrid Inf. Technol., vol. 4, **(2011)**, pp. 39-54.

[16] B. Borawski, J. A. Todd and J. Singh, "The influence of ductile interlayer material on the particle erosion resistance of multilayered TiN based coatings", Wear, vol. 271, **(2011)**, pp. 2890-2898.
[17] T. Brosh, H. Kalman and A. Levy, "Accelerating CFD-DEM simulation of processes with wide particle size distributions", Particuology, vol. 12, **(2014)**, pp. 113-121.
[18] A. Jovanović, M. Pezo, L. Pezo and L. Lević, "DEM/CFD analysis of granular flow in static mixers", Powder Technol., vol. 266, **(2014)**, pp. 240-248.
[19] J. Lindner, K. Menzel and H. Nirschl, "Simulation of magnetic suspensions for HGMS using CFD, FEM and DEM modeling", Comput. Chem. Eng., vol. 54, **(2013)**, pp. 111-121.
[20] M. H. Zhang, K. W. Chua, F. Wei and A. B. Yu, "A CFD-DEM study of the cluster behavior in riser and downer reactors", Powder Technol., vol. 184, **(2008)**, pp. 151-165.

